Volume 51
Number 18
14 May 2022
Pages 6981-7364

Dalton Transactions

An international journal of inorganic chemistry

rsc.li/dalton

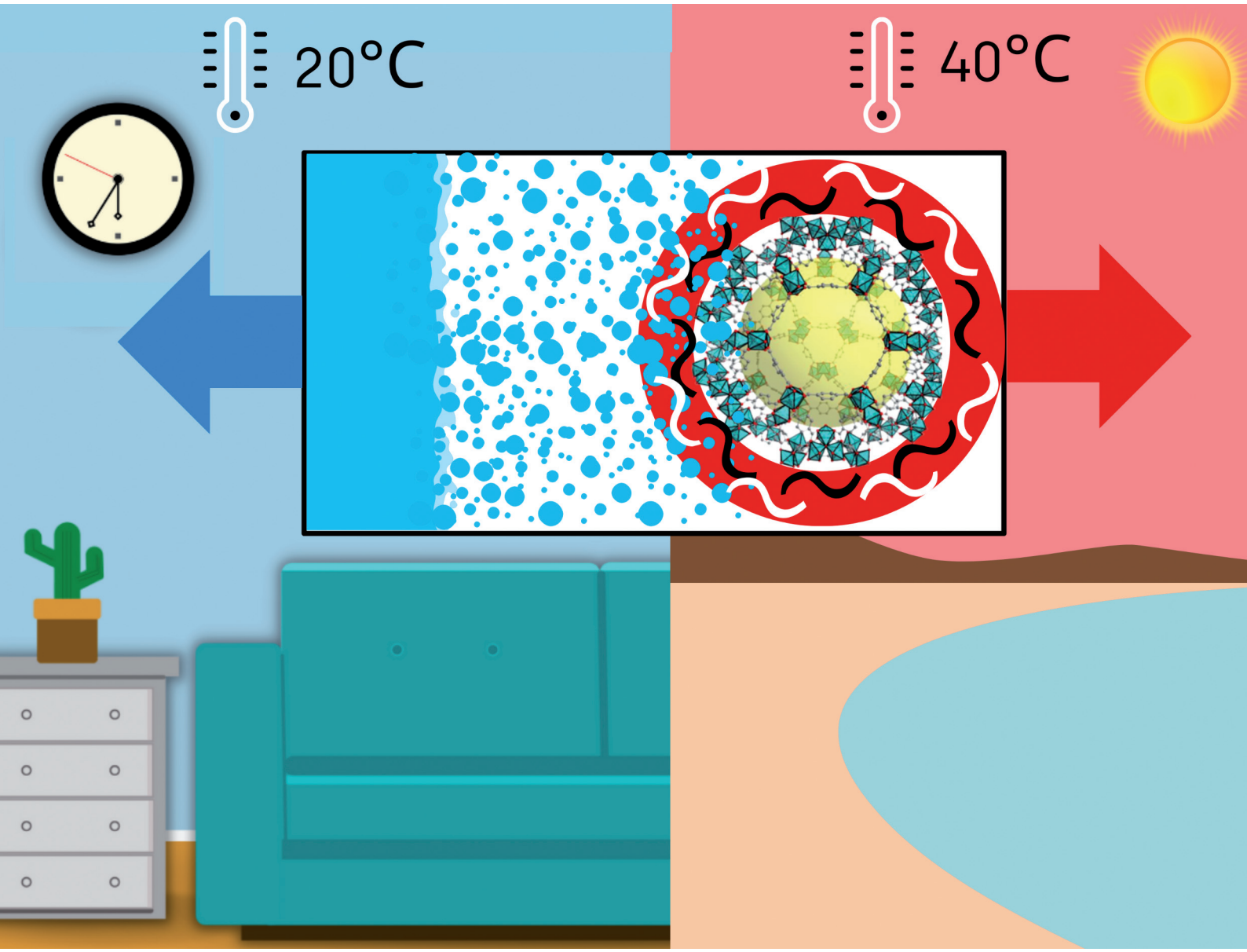

ISSN 1477-9226

ROYAL SOCIETY OF CHEMISTRY

PAPER

Tatsiana Shutava, Christoph Janiak *et al.*
Metal organic framework/polyelectrolyte composites for water vapor sorption applications

Dalton Transactions

ROYAL SOCIETY OF CHEMISTRY

PAPER

Cite this: *Dalton Trans.*, 2022, **51**, 7053

Metal organic framework/polyelectrolyte composites for water vapor sorption applications†

Tatsiana Shutava, *‡[a] Christian Jansen,‡[b] Kanstantsin Livanovich,[a] Vladimir Pankov[c] and Christoph Janiak*[b]

Received 18th February 2022,
Accepted 27th March 2022

DOI: 10.1039/d2dt00518b

rsc.li/dalton

Metal–organic framework (MOF) core particles of MIL-101(Cr), aluminum fumarate (Basolite® A520), MIL-53-TDC, zirconium fumarate, and UiO-66 were modified by adsorption of thin polyelectrolyte (PE)-based shells without deterioration of their crystal structure. By applying different PEs and depositing a single layer (MOF/PE) or one to three layer-by-layer assembled bilayers (MOF/LbL), the mass percent of shell material in the composite was varied from 0.6–2.5% to 50%. Under a constant relative pressure of water vapor, the moisture uptake by a MOF/PE and a MOF/LbL is rather comparable with its S-shaped curvature to that of pristine MOFs. The relevant differences, such as a shift of the ascending adsorption part to lower/higher relative pressure or an increase/decrease in water uptake in selected regions, are associated with the core–shell structure and related to the morphological changes of the MOF powders. The hydrophilic surface promotes the formation of liquid menisci at the points of contact between particles and accelerates the moisture uptake and loss. A decrease in water sorption under an atmosphere with high humidity by some composites can be associated with the inhibition of liquid water condensation by the more hydrophobic shells.

1. Introduction

Since the first metal–organic frameworks (MOFs) were synthesized, the interest in these porous crystalline materials has been steadily increasing.[1–6] MOFs are 3D coordination networks built of metal ions or metal clusters (nodes) linked by rigid polydentate organic ligands in such a way that a homogeneous one-, two- or three-dimensional spatial structure containing voids–potential pores is formed.[7–9] Due to their structure, MOFs have a tremendous specific surface area and can exchange small guest molecules with the surrounding. Until now, MOFs are being investigated as catalysts[2,4] and materials for storage and separation of gases,[5,6,10] humidity sorbents in harvesters of atmospheric water, air-conditioners, environmentally friendly heating and cooling technologies based on the sorption–desorption cycle of water vapor,[1,3,11–14] and humidity sensors.[15] The devices based on MOF utilizing sorbents can effectively capture water at low (below 30%) atmospheric humidity and further use solar energy or other secondary heat sources to regenerate the sorbent. Model units operating in arid climates (10–30% humidity, dew point below zero) can produce 0.25 L of water per 1 kg of MOF in one daily cycle.[16,17]

For practical applications, finely dispersed and microcrystalline MOF powders have to be mixed with polymeric or inorganic binders and molded into pellets, pressed into tablets or granules with a high percentage of the porous material, aiming to facilitate material handling and avoid the formation of dust particles.[18–21] Various approaches have been used to obtain MOF/polymer composites, for example, the inclusion of 35–75 wt% MOF into the macroporous matrices of polyacrylonitrile and poly-*N*-isopropyl acrylamide or resorcinol-formaldehyde xerogels.[18–20] Despite the achieved high mechanical stability, the incasing of MOF in polymer matrices often leads to a significant loss of its porosity and loading capacity, as well as an increase in the time period required to complete one adsorption/desorption cycle.[18–23] The reasons are the hydrophobicity and prolonged swelling of the polymer matrix material, its low water sorption capacity, and limited diffusion of water molecules through the polymer. Recent work in the shaping of MOFs has tried to develop procedures, such as freeze-casting or phase-separation techniques to prevent such loss of porosity.[24–26]

A distinctive feature of this work is the combination of MOF nano/microparticles and hydrophilic polymers bearing charged groups, that is polyelectrolytes. Those are polycations containing quaternary or protonated primary amino groups,

[a]*Institute of Chemistry of New Materials, National Academy of Sciences of Belarus, 36 F. Skaryna St., Minsk 220141, Belarus. E-mail: shutova@ichnm.by*
[b]*Institut für Anorganische Chemie und Strukturchemie, Heinrich-Heine-Universität Düsseldorf, 40204 Düsseldorf, Germany*
[c]*Belarusian State University, 4 Nezavisimosti Av., Minsk 220030, Belarus*
†Electronic supplementary information (ESI) available. See DOI: https://doi.org/10.1039/d2dt00518b
‡Both authors contributed equally.

such as poly(diallyldimethylammonium chloride) (PDDA), polyallylamine hydrochloride (PAH), polyethyleneimine (PEI), and chitosan (CH), and polyanions containing carboxy or sulfo groups, for example polyacrylic (PAA), carboxymethyl cellulose (CMC), polystyrene sulfonic acid sodium salt (PSS), dextran sulfate (DexS) (ESI, Fig. S1†). Typical polyelectrolytes are soluble in aqueous solutions and readily adsorb the surfaces of substrates with different geometries, including micro/nanoparticles and porous membranes. If the sequential adsorption of pairs of oppositely charged polyelectrolytes is repeated multiple times using the layer-by-layer (LbL) assembly method, a thin continuous film is formed on the surface of macroobjects, while each nano/microparticle envelops individually in a thin semipermeable shell.[27–29] The electrostatic interaction of adsorbing components of the coating is the main driving force of layer-by-layer assembly; however, in some cases, hydrogen bonds and other types of interactions contribute considerably.[30–33]

The thickness of the LbL film or shell is controlled with nanometer accuracy by simply changing the number of polycation/polyanion bilayers (n) and the conditions of their formation. It can be varied from 1–2 nm to several hundreds of nanometers by performing the required number of adsorption cycles.[30,35–44] By changing the pH, ionic strength, concentration of solutions and molecular weight of polyelectrolytes, the structure and surface properties of a coating are manipulated to achieve its linear or exponential growth.[29,41]

An important aspect of the preparation and application of polyelectrolyte films is their tendency to be saturated with water in both the liquid and gas phases. The mass fraction of water in polyelectrolyte layers in contact with an aqueous solution can reach 90% and depends on the polymers used and preliminary drying.[41,42] The average pore diameter of wet $(PAH/PSS)_n$, n = 7–10 multilayer films experimentally determined by NMR cryoporometry is 1.2–1.5 nm. The inner layers adsorbed on the substrate are tightly packed, while larger pores appear as a result of the loose packing of polymer outer layers with increasing n.[45] LbL-based shells in solution are permeable for water, ions, and small molecules; the diffusion coefficient of sucrose, glucose, methanol, and glycerin in multilayers is in the range of $(0.52–1.56) \times 10^{-9}$ m^2 s^{-1}.[44] The permeability of polyelectrolyte films for macromolecules with a molecular weight of more than 5 kDa depends on pH, temperature, and other factors.[29,41]

At the same time, the swelling of dry multilayer coatings in contact with the gas phase with a given partial pressure of water vapor (p/p_0), or relative humidity (RH), and its effect on the characteristics of the films are of practical importance.[46–51] The degree of LbL film swelling depends on the nature of the polyelectrolytes used, the conditions of layer preparation, and other factors. For example, for $(PAH/PAA)_n$ films, the relative increase in mass ranges from 1.1 to 1.35 at 80% humidity, depending on the pH value used upon film adsorption.[46] For $(PAH/PSS)_n$, n = 6–12, the percentage of water in the film reaches 30–50% and depends on the number of bilayers.[48] The swelling coefficient of thin multilayer films of poly(methacrylic acid) and poly-2-(dimethylamino) ethyl methacrylate chloride increases from 1.65 to 1.87 with an increase in the adsorption time of each layer from 3 to 25 min.[49] The water uptake by $(PDDA/PSS)_n$ and $(chitosan/dextran\ sulfate)_n$, n = 3 films at ambient temperature from gas phase with p/p_0 = 0.97 is 220 ± 10 and 380 ± 10 mg g^{-1} with ~a 15 min saturation time.[52]

The data on the effect of surface charge on LbL film swelling are contradictory. In ref. 46, it was shown that the positive electrostatic charge of the outer layer promotes swelling of the film, while in ref. 48 the degree of swelling of negatively charged films with the outer layer of PSS was 5–10% higher. A characteristic feature of multilayers $(PAH/PAA)_n$ prepared at two different pH values is a small hysteresis of the water sorption/desorption cycle,[46] while it is completely absent for common interpolyelectrolyte complexes. The diffusion coefficients of water from the gas phase into individual polyelectrolyte films (PSS and PAA), interpolyelectrolyte complex membranes and LbL films are within the range of 10^{-14}–10^{-6} cm^2 s^{-1} and affected by the thickness of the layer and temperature.[47,52–54]

Among the important features of LbL films that are relevant to the topic discussed here are the high water sorption capacity comparable to that of most MOF powders, the almost linear dependence of it on p/p_0, and the short saturation period.

In recent years, some attempts have been made to combine the advantages of MOFs and polyelectrolyte LbL films in one material. One of these approaches is the preparation of composites with high ion-exchange capacity *in situ* by polymerization of the corresponding monomers in MOF.[55,56] MOFs of the zeolite-imidazole type (ZIF) have been used as water-soluble cores for LbL microcapsules with pronounced edges.[57,58] Small molecules with therapeutic activity and contrast agents are effectively incorporated into nanosized MOFs coated with a polyelectrolyte shell.[59] However, the effect of polyelectrolyte shells on the water sorption characteristics of MOF/polyelectrolyte composites has not been investigated yet.

We report a new approach to control the water vapor sorption properties of MOF powders, namely by adsorption of a hydrophilic polyelectrolyte layer (MOF/PE) or a multilayer shell (MOF/LbL) on the surface of the MOF (Fig. 1). Due to the double compartment porous structure, the composite powders consisting of a MOF core and a polyelectrolyte shell are envisioned to have improved water sorption capacity and fast sorption/desorption cycle kinetics.

2. Experimental section

2.1 Materials and methods

Polycations [chitosan (ChH, 450 kDa, degree of deacetylation (DD) 75%, poly(diallyldimethylammonium chloride) (PDDA, 100–200 kDa), polyallylamine hydrochloride (PAH, 58 kDa), polyethyleneimine (PEI, 60 kDa)] and polyanions [polystyrene sulfonate sodium salts (PSS, 70 kDa), polyacrylic acid (PAA, 2.5 kDa), carboxymethyl cellulose (CMC, 250 kDa), dextran sulfate (DexS, 6.5–10.0 kDa and DexH, >500 kDa), and

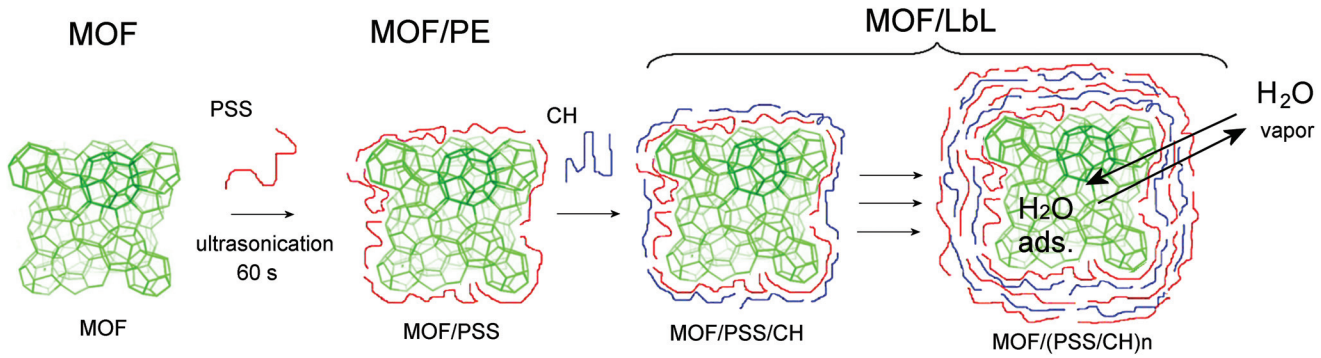

Fig. 1 Scheme of the formation of a shell on the surface of a MOF powder using adsorption of single polyelectrolyte layer (MOF/PE) or layer-by-layer shell (MOF/LbL) with the exemplifying polymers, polystyrene sulfonic acid (PSS) and chitosan (CH).

κ-carrageenan (CAR, 5–25 mPa s, 0.3% in H_2O, 25 °C)] were obtained from Sigma-Aldrich and used to form mono- and multilayer polyelectrolyte shells on MOF particles. Chitosan of low molecular weight (CH, 18 kDa, DD 75%) and two hydrophilic graft-copolymers of CH with 5 kDa polyethylene glycol (CH-PEG) and 6 kDa dextran (CH-DEX) were synthesized.[60] Polyallylamine hydrochloride labeled with fluorescein isothiocyanate (PAH-FITC) was synthesized from PAH of 18 kDa and FITC as described.[60]

All chemicals for MOFs syntheses were used as received from suppliers.

A Zetasizer NanoZS (Malvern) analyzer was used for measuring the ζ-potential and the hydrodynamic diameter of MOF particles. The value of the number average hydrodynamic diameter (d_N) and polydispersity index (PDI) of each sample was obtained from three independent measurements using the instrument software. To obtain the porosity of the MOF powders, nitrogen (purity 99.9990%) physisorption isotherms were measured with *ca.* 20–50 mg of the MOF sample using an Autosorb-6 from Quantachrome at 77 K, thermostated with liquid nitrogen. Before each nitrogen or water sorption measurement, the samples were activated under vacuum (1×10^{-3} mbar) at 373 K for 3 h. Water vapor sorption isotherms were measured volumetrically using a Quantachrome VSTAR vapor sorption analyzer (model number Vstar4-0000-1000-XS) at 293 K. For water uptake as a function of relative pressure of water vapor *V-Star*, a Quantachrome analyzer was used.

The apparent Brunauer–Emmett–Teller (BET) surface areas were calculated from the nitrogen physisorption isotherms. All surface areas (BET) were calculated from five adsorption points by applying Roquerol plots ($r > 0.998$). We note that the microporous MOF surface areas derived from type I isotherms should be regarded as "apparent S (BET) values" since "the BET-area derived from a type I isotherm must not be treated as a realistic probe accessible surface area" but it "represents an apparent surface area, which may be regarded as a useful adsorbent fingerprint".[61] The density functional theory (DFT) calculations for the pore size distribution curves were done with the native NovaWin 11.03 software using the "N_2 at 77 K on carbon, slit pore, non-local density functional theory (NLDFT) equilibrium" model for nitrogen. In addition, none of the present DFT kernels for "N_2 on carbon" reflect the surface properties of a MOF material. The numbers can be used for the comparison of similar materials but must not be taken as exact values for the pore sizes or surface areas of MOFs. In the absence of MOF-specific kernels, the N_2 on carbon kernels with different pore types is frequently used to study the surface properties of the MOFs.[62]

Powder X-ray diffractometry (PXRD) was performed at ambient temperature using a *D2 Phaser* (Bruker AXS, Karlsruhe, Germany) using Cu-K_α radiation (λ = 1.54182 Å) between $5° < 2\theta < 50°$ with a scan rate of 0.0125 s^{-1} (300 W, 30 kV, 10 mA). Analyses of the diffractograms were carried out with the Match 3.11 software.

2.2 QCM measurements of water vapor uptake by MOF/LbL powders

The time-related parameters of water uptake by MOFs were determined by the quartz crystal microbalance technique using a QCM200 Stanford Research System instrument equipped with quartz resonators with a gold working surface and a nominal frequency of 5 MHz. Before the experiment, the resonators were cleaned for 5 min at 75 °C with a mixture of water, 25% NH_3 solution, and 30% H_2O_2 solution taken in a volume ratio of 3 : 1 : 1, washed 4–5 times with distilled water and dried in an argon flow. The unloaded resonator was placed in an open cell of the device, which allowed the resonator surface to contact the environment, and its resonant frequency (F_0) and dynamic resistance (R_0) were determined at a given temperature and relative humidity over dry KOH (RH 6–10%). The temperature and humidity near the resonator surface were determined using a TKA-PKM thermohygrometer.

The temperature dependence of the frequency and the dynamic resistance of an unloaded resonator are due to the fundamental properties of quartz and depend on the shape of the quartz crystal or the type of its cut.[63] When the temperature increases from 23 to 34 °C, the F_0 value of the resonator decreased by 10–15 Hz, and the dynamic resistance R_0 by no more than 0.5 Ohm. At constant temperature, humidity does not affect the oscillation frequency of the unloaded resonator

(the change does not exceed 1 Hz), while the resistance changes less than 1.5 Ohm when RH changes from 6 to 90%.

The MOF under investigation (~10 μg) was applied on the planar surface of the resonator in the form of a diluted suspension in water, pretreated with ultrasound for 2 min, and dried over KOH at room temperature for 1 h. The cell with the resonator was placed in a chamber with controlled RH and temperature and kept over KOH until a constant value of frequency (F_{KOH}) was established.

The mass of dry deposit on the surface of the resonator (m_f) was calculated using the Sauerbrey equation:[63]

$$m_f = -\Delta F/C, \quad (1)$$

where $\Delta F = F_{KOH} - F_0$ is the change in frequency, Hz; m_f is the deposit weight per unit area, μg cm^{-2}; C is the sensitivity factor equal to 56.6 Hz cm^2 μg^{-1} for a quartz resonator with a frequency of 5 MHz. The sample mass on the resonator surface was 2.4–5.2 μg cm^{-2}.

The specified RH of the medium in the thermostat was maintained by using a saturated solution of the corresponding salt.[64] At a constant temperature, the cell with the resonator was sequentially placed over saturated salt solutions (LiCl, $MgCl_2$, NaBr, NaCl, KCl, and K_2SO_4) in the order of increasing partial pressure of water vapor, after which the relative humidity was successively decreased, ending with a medium over dry KOH. After reaching the constant temperature and relative humidity, as well as the equilibrium values of the frequency and dynamic resistance of the resonator, they were determined with one decimal point accuracy. When calculating the saturation of MOF powders at different humidity (q_e), the resonator with the deposit was sequentially placed over dry KOH (F_0^{RH}) and saturated salt solutions, and after establishing a constant value, the oscillation frequency of the resonator with the MOF deposit at a given humidity (F_e^{RH}) was determined.

The kinetics of water sorption by the MOF deposit was investigated by rapidly moving the resonator from the atmosphere over dry KOH (RH < 10%), which corresponds to the initial values of frequency and resistance F_{to} and R_{to}, into a chamber saturated with water vapor (RH = 90%) and recording the F_t and R_t values of the resonator in time. The water content of MOF at time t (q_t) was used for the calculation of the kinetic parameters of the process. Desorption of water vapor was studied in a similar way.

The water content in the powder $q_{e,t}$ (in g/g) was calculated using the formula:

$$q_{e,t} = -\Delta F_{e,t}/(C \cdot m_f), \quad (2)$$

where $\Delta F_e = F_e^{RH} - F_0^{RH}$ and $\Delta F_t = F_t - F_{to}$.

The changes in the resonant frequency and resistance due to water absorption by a deposit are recalculated relative to the values of the semi-dry deposit above KOH (RH is equal to or less than 10%). As a result, despite the amount being relatively small, water that is already present in the deposit at the lowest experimental humidity is not taken into account.

2.3 Synthesis

2.3.1 Metal–organic frameworks. Metal–organic frameworks (MOF) were synthesized as described in detail elsewhere.[65–69] MIL-101(Cr) was synthesized according to Chang *et al.* by microwave-assisted synthesis. The reaction mixture was loaded in a Teflon autoclave, sealed and placed in a lab microwave oven. Purification and drying were done using the reported method.[65] Aluminum fumarate (Al-fum) was synthesized according to the BASF patent at 60 °C and was also purchased from BASF as Basolite® A520.[66] MIL-53-TDC was synthesized according to Tannert *et al.*[67] The aluminum source was $NaAlO_2$ and the synthesis was carried out under reflux at 135 °C for 24 h. Zirconium fumarate (Zr-fum) was synthesized according to Zahn *et al.*[68] The used modulator was acetic acid and the synthesis was achieved at 120 °C for 24 h. UiO-66 was synthesized according to Shearer *et al.*[69] The used modulators were hydrochloric acid and HCl/H_2O and the synthesis conditions were 100 °C for 24 h.

2.3.2 Preparation of MOF powders modified with polyelectrolyte single layer or shell. The MOF powder was dispersed in water at a concentration of 2 mg mL^{-1} using a *Sapphire* ultrasonic bath for 20 s, then 0.25 mg of polyelectrolyte per 1 mg of MOF was added as an aliquot of 10 mg mL^{-1} polyelectrolyte solution and the suspension was additionally sonicated for 60 s and left for 10 min at room temperature. The particles coated with the polyelectrolyte layer were separated by centrifugation (a *ZH36, Hermle* centrifuge, 1000*g*, 10 min), washed once with water to remove unadsorbed polyelectrolyte, and redispersed in water. In a similar way, shells were formed on the surface of the particles, consisting of 1–6 layers of polyelectrolyte (0.5–3.0 bilayers). The dispersions of MOFs modified with a single polyelectrolyte and a shell of required number of layers in water were frozen at −20 °C and lyophilized.

In an additional series of experiments, 20 mg of selected MOF powder was suspended in 9 mL of water and 0.1 mg mL^{-1} PSS solution was added dropwise as 150 μL aliquots to obtain a low ratio of m_{PSS} and m_{MOF}. The mixture was carefully shaken. After 10 min, 25 μL of it was withdrawn with a pipette, resuspended in 2 mL of water, and used for the measurements of the hydrodynamic diameter and ζ-potential of MOF particles.

Polyelectrolyte shells consisting of three bilayers of PSS/PDDA or DexH/ChH were formed on Al-fum in a 0.2 M sodium chloride solution. A 4 mg mL^{-1} suspension of Al fumarate was mixed with an equal volume of 2 mg mL^{-1} of PSS or DexH solution, sonicated for 1–2 min, and left at room temperature for 30 min. The resulting particles with a polymer layer adsorbed on them were separated by centrifugation, washed 2 times, and dispersed in 0.5 mL of a 0.2 M NaCl solution. The chitosan or PDDA layer was formed in a similar way.

2.3.3 Preparation of MOF/thick LbL composite. A thick shell consisting of two PSS/PDDA bilayers was formed on the particles of Al fumarate powder using excessive amounts of polyelectrolytes: a MOF sample weighing ~0.08 g was dispersed in 1 mL of water, 0.02 g of PSS was added as a 10 mg

mL^{-1} solution, and the mixture was treated by ultrasound for 60 s. Without intermediate washing, 0.02 g of PDDA was added to the mixture as a concentrated aqueous solution. The procedure of PSS/PDDA deposition was repeated. The MOF particles with a thick polyelectrolyte shell were separated by centrifugation and dried at 110 °C in air. The calculated ratio of the mass of polyelectrolyte shell to the mass of MOF is 1 : 1. The composite sample was stored at RH = 97% in a sealed desiccator overnight and the water content of the sample was characterized using a MAX 50 Radwag moisture analyzer by heating to 80 °C to evaporate water adsorbed by the composite. The kinetics of water sorption by the composite powder was measured at 23 °C and an ambient relative humidity of 70%.

3. Results and discussion

The criteria for the selection of MOF powders for modification with a polyelectrolyte shell were high chemical stability and hydrolytic resistance, large values of specific surface area (above 400 $m^2\ g^{-1}$) and water vapor capacity (at least 500 mg g^{-1} or higher), as well as an S-shaped water sorption isotherm with an inflection point of water uptake lower than $p/p_0 = 0.5$. The chosen MOFs MIL-101(Cr), aluminum fumarate (Basolite® A520), MIL-53-TDC, zirconium fumarate, and UiO-66 were all well-investigated for their water sorption behavior before as noted in the given references.[34,67,70–74] A brief structure description of these MOFs is given in the ESI, Table S2.† In the selected MOFs, the diameter of windows through which small molecules can penetrate the framework does not exceed 0.8–1.6 nm.

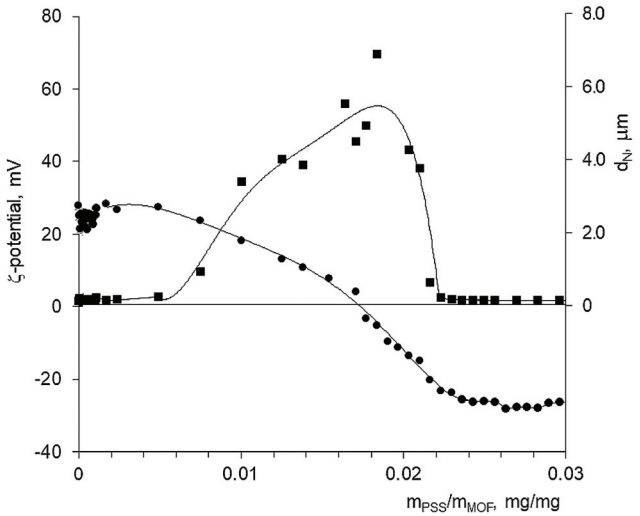

Fig. 2 Dependence of the ζ-potential and the hydrodynamic diameter (d_N) of particles of the MOF UiO-66 on m_{PSS}/m_{MOF}.

Table 1 ζ-Potential and the PSS-based neutralization and recharge points of MOFs

		m_{PSS}/m_{MOF}, mg g^{-1}	
MOF	ζ-Potential, mV	Zero charge	Recharge
UiO-66	27.9 ± 0.1	17.5	25.5
MIL-53-TDC	23.4 ± 1.1	4.0	13.6
Al fumarate	13.6 ± 0.1	2.4	6.2
Basolite®A520	7.4 ± 0.2	9.2	15.6
Zr fumarate	1.1 ± 0.1	—	4.3

3.1 Quantification of PE adsorption on MOF

By quantitative analysis of polyelectrolyte adsorption on porous MOF particles, we selected PSS as a strong polyelectrolyte that is fully charged in a wide range of pH.[75–78] Among the MOFs, UiO-66 and MIL-53-TDC are samples with high ζ-potential values; the two aluminum fumarate samples differ in particle size, Al-fum (2.3 μm) and Basolite® A520 (270 nm), with a moderate positive ζ-potential in the range of 5 to 15 mV, while Zr-fum has $\zeta \approx 0$. Fig. 2 shows the changes in the ζ-potential and hydrodynamic diameter of the MOF UiO-66 during a step-wise addition of negatively charged PSS. Upon increasing the m_{PSS}/m_{MOF} ratio, the negative charge of the particles increases. We assumed that PSS adsorbs quantitatively on MOF particles until a saturated polyelectrolyte layer is formed and a constant negative ζ-potential value is attained. PSS added over that amount remains dissolved in solution but does not cause an additional decrease of the ζ-potential. In the subsequent washing stage, this excessive PSS is removed but the adsorbed polyelectrolyte macromolecules remain on the surface electrostatically bound to it at numerous points.

As one can see from Table 1, the amount of PSS required to fully recharge the MOFs depends on the powder under investigation. The value is definitely related to the difference in their structure; however, for all studied MOFs, the recharge values do not exceed 25–26 mg g^{-1} MOF, or 2.5 wt%. At the same time, the water uptake by the MOF powders reaches usually a 20-fold higher value. The results obtained prove that the adsorption of polyelectrolytes on MOFs is not associated with their penetration into micropores but apparently occurs on the surface of particles. A higher recharge value for Basolite® A520 that has smaller particles as compared with the larger ones for Al fumarate confirms the outer surface–related adsorption of PSS.

To coat the MOFs, all polyelectrolytes were taken in excess (~0.25 mg per 1 mg MOF) and the unadsorbed polymer was removed after deposition of each layer by rinsing with DI water. Taking the PSS-based recharge value for different MOFs as an approximate mass of a single polyelectrolyte layer, one can estimate that the mass of an LbL shell that consists of 3 bilayers is less than 150 mg per 1 g of MOF, or 13 wt%.

Another value obtained in this series is the zero charge m_{PSS}/m_{MOF} ratio needed to neutralize the positive charge of the pristine MOF particles. It is reasonably smaller than the recharge PSS/MOF ratio. Obviously, in the vicinity of the zero-charge ratio, the MOF particles are most agglomerated in a dispersion due to the disappearance of electrostatic repulsion (Fig. 2). However, at such small polyelectrolyte-to-MOF ratios,

it is difficult to uniformly modify concentrated MOF dispersions.

A composite consisting of Al-fum particles coated with a thick $(PSS/PDDA)_2$ shell was also obtained by using LbL assembly without intermediate washing.[79,80] This technique precisely controls the weight fraction of the shell material by adding a predetermined, excessive in the given case, amount of polyelectrolyte in each step without separating it after adsorption. In the obtained MOF/thick LbL shell composite, the mass of the LbL shell is 50 wt%, or equal to the mass of the MOF cores.

3.2 Morphology of the MOF/PE and MOF/LbL powders

The SEM microphotographs of the selected MOFs modified with a single polyelectrolyte layer or an LbL shell are shown in Fig. 3. The shape and size of the particles of the different MOFs vary but all of them are faceted; those are typical of crystalline substances. The SEM images of pristine MOFs are given in the ESI, Fig. S3† for comparison. A single polyelectrolyte layer does not change the morphology of any other MOFs as illustrated in the ESI, Fig. S4† on the example of MIL-53-TDC coated with PAA, CMC, DexS, and CAR.

Due to high hydrophilicity, all MOF powders are easily dispersed in water, while the sedimentation of their suspensions depends on the size of the particles. The average hydrodynamic particle diameter of the pristine MOFs as determined by dynamic laser light scattering (DLS) ranges from 0.2 to 2.3 μm with a PDI value exceeding 0.3 (ESI, Fig. S5†), which is typical of polydispersed particles. In the process of sonication-assisted polyelectrolyte adsorption, MOFs with an average hydrodynamic diameter of less than 700 nm (such as MIL-101(Cr), MIL-53-TDC and Basolite®A520) tend to aggregate at varying degrees through the added PE shell; the polydispersity values of the PE-coated samples remain high. For the MOF Al fumarate, diameters of 2.3 and 2.0 μm and polydispersity values of 0.33 and 0.43 were found before and after single adsorption of polystyrene sulfonate on the MOF, indicating the negligible influence of the ultrasound-assisted PSS adsorption on the powder morphology.

The SEM images of the prepared Al-fum and commercial Basolite® A520 powders with LbL shells of different numbers of bilayers are shown in Fig. 3c and d (the additional SEM images are given in the ESI, Fig. S6†) and ESI, Fig. S7,† respectively. The effect of a shell consisting of one (polycation/polyanion) bilayer on the morphology of both powders is insignificant. For Al-fum powders with a three bilayer shell, the microparticles in dry powder have well-defined boundaries and fairly close sizes. According to the DLS data (ESI, Fig. S5†), the diameter of Al fumarate microparticles with a shell based on chitosan and its copolymers with polyethylene glycol and dextran decreases.

The thickness of a single adsorbed polyelectrolyte layer usually does not exceed 1–2 nm, while for a 3 bilayer shell it is typically less than 20 nm.[30,31,41–43,45] Due to the minimal dimensions and the absence of any staining, the adsorbed PE or LbL shells do not appear in the SEM images of the MOF powders. The presence of an LbL shell on the surface of the MOF particles was confirmed by using a dye-labeled polyelec-

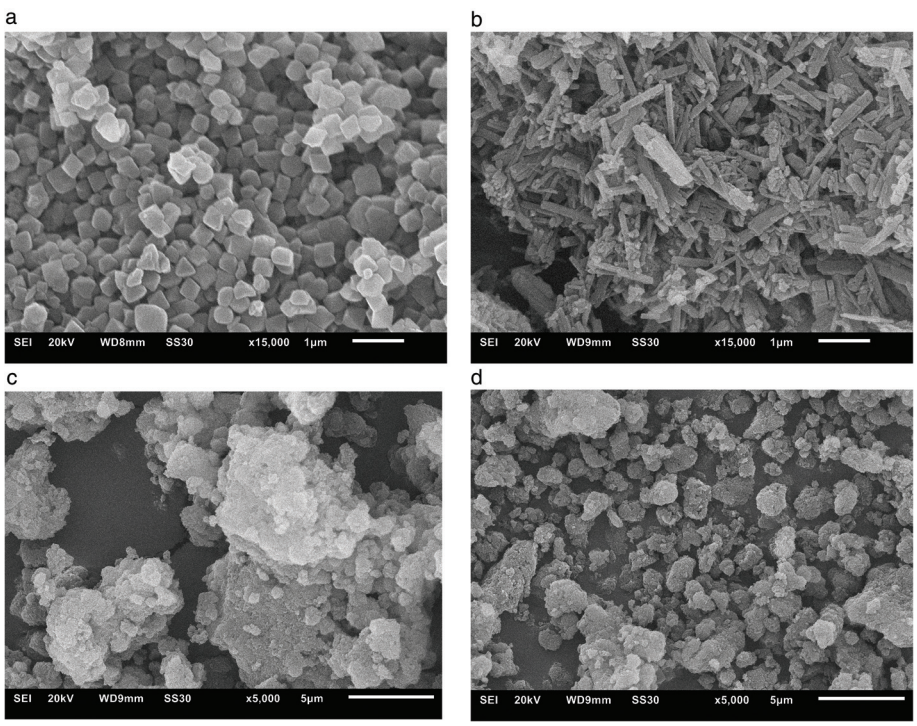

Fig. 3 SEM micrographs of MIL-101 (Cr) modified by PSS (a) MIL-53-TDC with PAA (b), Al fumarate modified with an LbL shell: PSS/CH (c) and $(PSS/CH)_3$ (d).

trolyte as one of the shell components. The images in transmitted and reflected light showing agglomerated Al-fum powder coated with a shell of PSS and FITC-labeled PAH are presented in the ESI,† Fig. 8. The location of the yellowish regions coincides with the spatial arrangement of the MOF particles confirming the inclusion of FITC-labeled polymer into a shell.

Most importantly, the MOFs have to retain their phase and crystallinity together with their porosity in the MOF/PE composites as assessed by PXRD and nitrogen porosimetry, respectively. The positions of the reflections in the PXRDs of the MOF/PE and MOF/LbL composites are in good agreement with the pristine MOF powders and their simulation (ESI, Fig. S9†) proving the unchanged phase and crystallinity. The diffractograms are not affected by the nature of the polyelectrolyte layer on the MOF surface. Since the adsorption of polyelectrolytes occurs under mild conditions (aqueous solutions of polymers with close to neutral pH, 25 ± 1 °C), the chosen MOFs do not degrade during the adsorption of polyelectrolytes in aqueous solutions.

The BET surface area of most PE or LbL modified MOF powders as evaluated by nitrogen sorption (Fig. 4) remains comparable to that of the unmodified MOF, and only in few cases decreases significantly. On the other hand, the surface area of MIL-101(Cr) treated with polycations (PDDA, PAH, and CH) and UiO-66 modified with PAA, as well as some aluminum fumarates with an LbL shell (PSS/CH and $(PSS/CH\text{-}DEX)_3$ for Al-fum; and PSS/PDDA and PAA/PDDA for Basolite®A520) were found to increase. Such an increase can occur through the formation of the added interface volume.

Two cases showing a significant decrease in the surface area were MIL-101(Cr)/PAA and MIL-53-TDC with PSS or DexS. Among the used polyelectrolytes, PAA and DexS were of low molecular weight (2.5 and <10 kDa, respectively). Since no aggregation of MIL-101(Cr) in solution was found after treatment with various polymers as confirmed by DLS measurements (ESI, Fig. S5†), the low BET surface area of MIL-101(Cr)/PAA reflects the filling of mesopores with oligomeric PAA molecules; for the PAA-modified MOF, the volume and surface of mesopores available for nitrogen adsorption decrease (ESI, Fig. S10†).

For MIL 53-TDC, there is a more complex situation. The BET surface area of the powders declines to various degrees after their modification with any negative polyelectrolyte (Fig. 4). The decrease is accompanied by both aggregation of nanoparticles (appearing as an increasing d_N and PDI in ESI Fig. S5†) and reduction of micropore volume (ESI, Fig. S10†). For the MIL 53-TDC/DexS powder, both these effects are intense and lead to a pronounced decrease in the BET surface. The SEM images of these modified MOFs (ESI, Fig. S4†) also show large agglomerates of MIL 53-TDC/DexS particles.

Nevertheless, for the overwhelming number of MOFs, single adsorption of the polyelectrolyte does not lead to a significant decrease in the specific surface area of the powders. A size comparison shows that the radius of gyration (R_g) of most polyelectrolytes with molecular weights above 20–30 kDa in water is several times larger than the half diameter of the micropore cage window and the interior space in most MOFs.[81–86] Thus, the micropores are inaccessible for penetration and localization in the polyelectrolytes in a random coil conformation. At the same time, they can adsorb on the inner surface of mesopores with a diameter of up to 50 nm and macropores forming a complete or partially filled layer of the adsorbate. Consistently, the higher the molecular weight and the corresponding value of R_g of the used polyelectrolyte, the less likely it adsorbs on the inner mesopore voids and affects

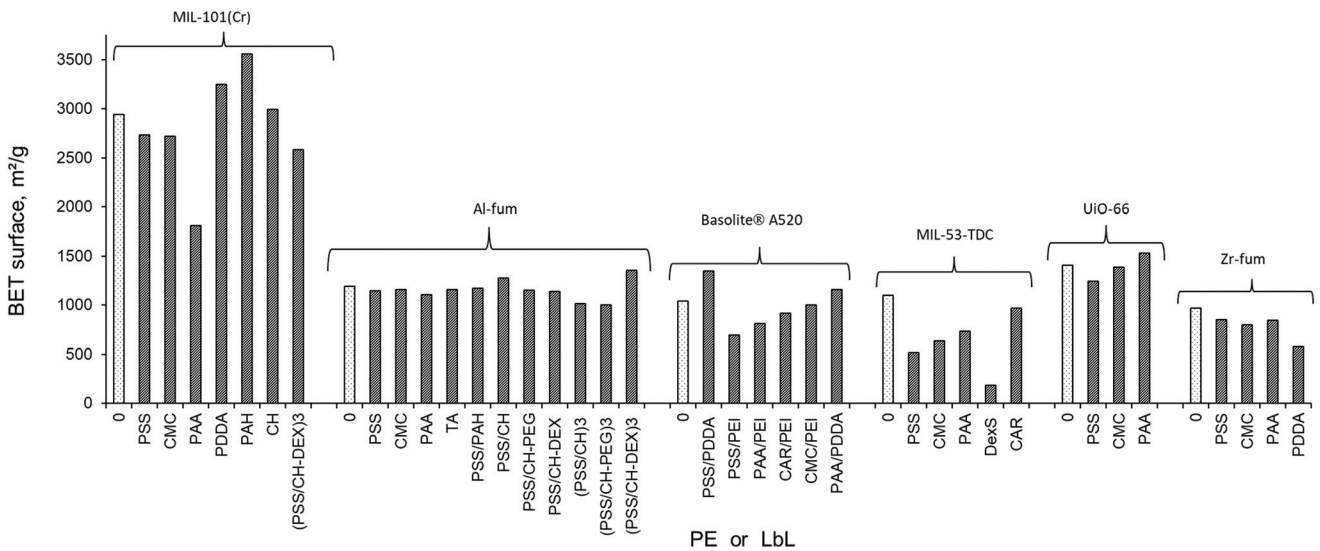

Fig. 4 Specific surface area of MOF powders modified by the adsorption of a single polyelectrolyte layer or LbL shell. At a surface area of 1000 m^2 g^{-1}, the error is assumed to be ±50 m^2 g^{-1}.

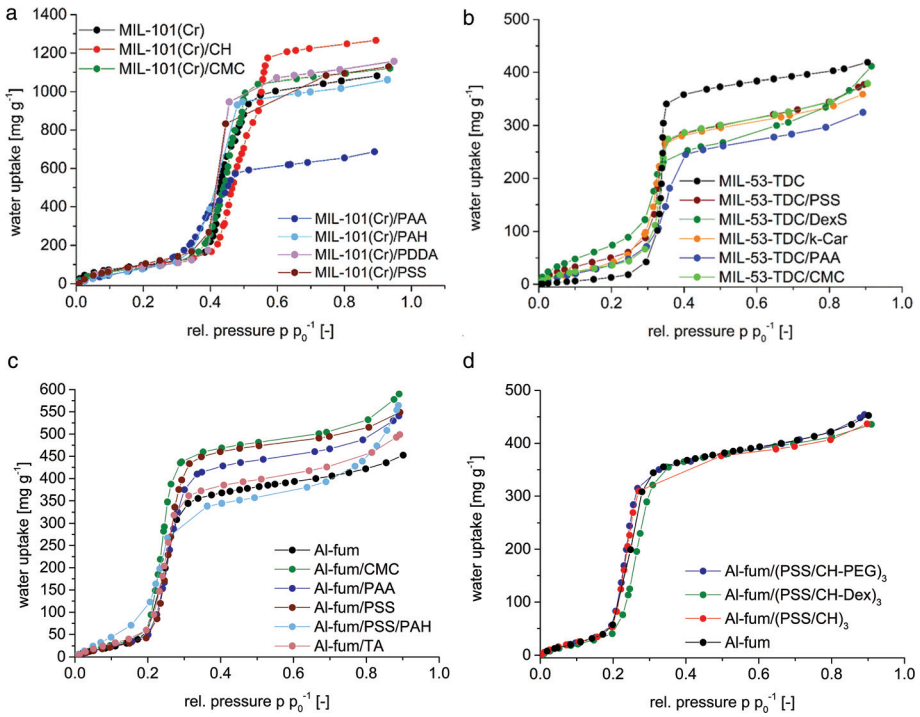

Fig. 5 Sorption isotherms of MOF/PE and MOF/LbL powders: (a) MIL-101(Cr), (b) MIL-53-TDC; and (c and d) Al fumarate.

the porosity-related properties of the powders. Therefore, unchanged sorption characteristics of modified MOFs can be expected.

3.3 Water uptake

The isotherms of water uptake by MOF, MOF/PE, and MOF/LbL powders against the relative pressure of water vapor are all S-shaped (Fig. 5 and ESI, Fig. S11†). Similar to the pristine MOFs, all modified powders retain the main sorption profile of the parent powders while there are some specific features brought upon by the adsorption of polyelectrolytes.

At first sight, the PE-modified MOFs of MIL-101(Cr), Al-fum and MIL-53-TDC seem to have the same low adsorption of water in the low relative pressure regions before the sharp incline and a sharp increase in water uptake, which is characteristic of the pristine MOF. A closer inspection shows the relevant differences, such as a shift in the ascending part to the lower/higher relative pressure (Fig. 6a) or an increase/decrease in water uptake in the selected regions (Fig. 6b).

A shift to 'earlier' uptake, that is to lower relative pressure, means that the composite has become more hydrophilic compared to the neat MOF. Such an earlier uptake is seen for MIL-101(Cr)/(PSS, CMC, PAA, PAH), all Al-fum/PE, and all MIL-53-TDC/PE composites.

A shift to 'later' uptake, that is to higher relative pressure, means that the composite has become more hydrophobic compared to the neat MOF. Such a shift to later uptake is brought about by chitosan to MIL-101, along with an increase in the uptake capacity after the inflection point. For UiO-66 also, a shift to later uptake upon composite formation takes place, together with an increase in the uptake capacity under a humid atmosphere. The synthesized UiO-66 is a hydrophilic MOF with most of its uptake below p/p_0 = 0.2. Relative to UiO-66, the used polymers are more hydrophobic and therefore shift the uptake to higher p/p_0. An interesting case is Zr-fum (MOF-801) which has the same structure as UiO-66 and is even more hydrophilic since a significant part of the water uptake is concluded at p/p_0 = 0.1.[74] Yet, the uptake pressure in Zr-fum is essentially slightly shifted with relatively more hydrophobic PE shells. The effect of the increased uptake capacity is noticeable only for Zr-fum modified with PSS, which is usually considered as more hydrophobic PE than CMC or PAA. Due to the high water uptake under an arid atmosphere, even as a composite, the MOF Zr-fum can be an excellent desiccant for high-precision optical and electronic equipment.

For MIL-101(Cr) with the $(PSS/CH\text{-}Dex)_3$ LbL coating, there is also a light shift to 'earlier' water uptake as compared to the unmodified MOF. LbL-coated Al-fum and Basolite®A520 experience a light hydrophilic shift similar to the parent Al-fum/PE powders. A decrease in water uptake after the steep increase for MIL-101(Cr)/(PSS/CH-Dex) and for all Basolite/LbL composites is quite noticeable, while all Al-fum/LbL composites show little, but also negative, change in uptake capacity.

The effect of modifications on water uptake by MOF/PE and MOF/LbL at low partial water pressure is associated, first of all, with the high water sorption capacity of the individual polyelectrolytes and based on the LbL shells. For example, for $(PDDA/PSS)_n$ and $(CH/DexS)_n$ layers, it can be as high as ~50 mg g^{-1} at p/p_0 = 0.2; the value is comparable with that for some MOFs under an arid atmosphere.[52] The MOFs with high

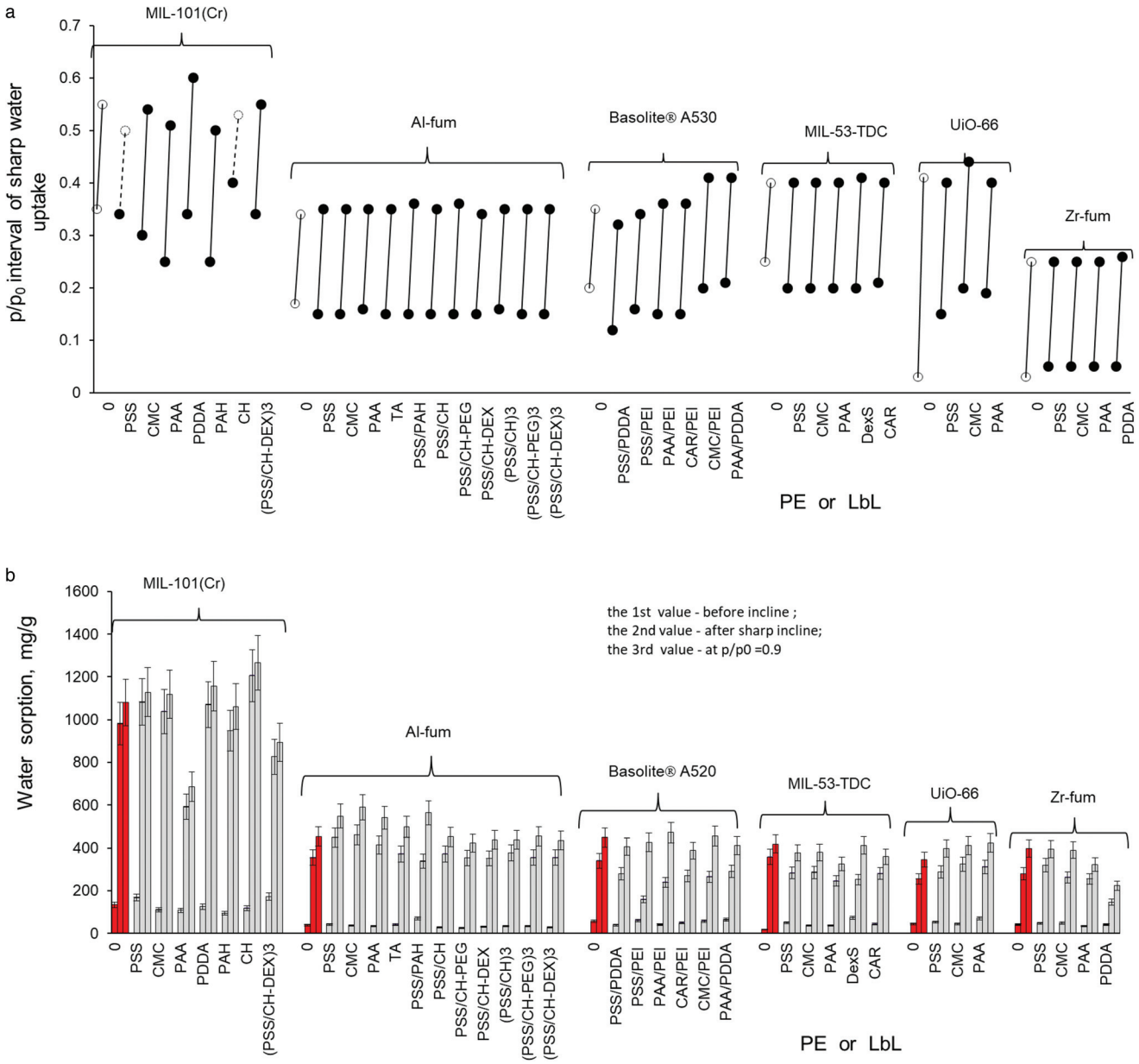

Fig. 6 Steep rise in the p/p_0 interval of the S-shaped water uptake curve (a) and the corresponding water uptake. (b) The values are given in the following order: before and after the sharp incline and at p/p_0 = 0.9 for MOF/PE and MOF/LbL powders.

polyelectrolyte adsorption per layer, such as UiO-66, Basolite® A520, and MIL-53-TDC (Table 1), are expected to be more prone to increased uptake below their inflection point than Zr-fum and Al-Fum.

At the same time, a light or reverse effect of chitosan-based shells is apparently related to the small water adsorption capacity of chitosan at low partial water pressure[87,88] as compared with other polyelectrolytes; moreover, its replacement with a copolymer or complexation with PSS does not improve the water vapor adsorption.

For the discussion of water uptake capacity by different MOFs, the technologically important value lies at the end of the steep rise of the S-shaped water uptake curve, which is at $p/p_0 \approx 0.55$ for MIL-101(Cr), ≈0.35 for Al-fum, ≈0.4 for MIL-53-TDC and UiO-66 and ≈0.25 for Zr-fum. The corresponding water uptake values are given in the middle columns of the diagram for each composite in Fig. 6b.

The changes in the water uptake capacity and BET surface area of the modified MOFs do not always correlate (compare Fig. 4 and 6b). The significant decrease in surface area which was seen for MIL-101(Cr)/PAA is also followed by a decrease in water uptake. Not just MIL-53-TDC with PSS or DexS shows a noticeable decrease in surface area but all other MIL-53-TDC/PE composites and Zr-fum/PDDA also exhibit a sizable decrease in water uptake, albeit the decrease in their surface area is minor. On the other hand, Al-fum/PE and UiO-66/PE,

in which the surface areas vary slightly around one of the pristine MOFs, exhibit a remarkable increase in water uptake. Most likely this is due to the MOF–PE interaction at the nanoscale and the added MOF–PE interface volume. An indication of the latter is the strong increase in the slope of the water sorption isotherm above $p/p_0 > 0.6$, that is, with an even steeper slope than that of the neat MOF (Fig. 5c and ESI, Fig. S11c†).

For LbL-coated samples, the strong increase in the slope of the water sorption isotherm under a humid and fog atmosphere (above $p/p_0 > 0.6$) is more typical than that for the neat MOFs or MOF/PE composites (see the isotherm for Al-fum/(PSS/PAH) in Fig. 5c and those for Basolite® A520/LbL in ESI, Fig. S11b†). In several cases, it compensates for the decrease in adsorption under mild humidity and sometimes increases the water uptake value above that of neat MOFs. For example, the composite with a thick LbL shell also shows increased water sorption characteristics (420 and 440 mg g^{-1} in the first and second sorption cycles at 23 °C, $p/p_0 = 0.7$, respectively) as compared with pristine Al-fum (415 mg g^{-1}). At the same time, the water sorption capacity of planar $(PSS/PDDA)_n$ films under these conditions does not exceed 100 mg g^{-1}.[52] This also proves the non-additive effect of the polyelectrolyte shell on water uptake by the composite.

3.4 Water vapor uptake kinetics

The kinetics of water vapor uptake by two MOFs, Al-fum and MIL-53-TDC, and two Al-fum/LbL composites were followed by the QCM technique. Typical changes in frequency F_t and motional resistance R_t of a resonator with a thin deposit of MOF composite particles on its surface while it is in the chamber with alternately changing from 10 to 90% humidity are shown in ESI, Fig. S12.† A decrease in F_t (directly proportional to adsorbed mass) and an increase in R_t (characterizing viscoelastic properties of deposit) of the resonator at RH 90% correspond to the sorption of water vapor by immobilized MOF particles. At RH 10%, an increase in F_t and a decrease in R_t are observed due to water desorption. The process of water sorption at temperatures of 25–47 °C is reversible for both unmodified and modified MOFs at least within four consecutive adsorption–desorption cycles.

Calculated on the basis of ΔF_t, the values of apparent water uptake and loss by MOF Al-fum and Al-fum/LbL composite as a function of time are shown in Fig. 7. Regardless of temperature, the kinetic curves of water adsorption by MOF-based powders consist of two sections: a short initial stage, where up to 90% of the mass change occurs due to fast water sorption, and a long smoothly sloping section which can be apparently associated with the slow relaxation of the deposited structure (Fig. 7a). The shape of the water vapor desorption curves (Fig. 7b) indicates that the process proceeds in several stages, more pronounced at 25 °C.

The experimental values of water uptake (q_e) obtained after the exposure of arid MOFs to $p/p_0 = 0.9$ for 15 min are summarized in Table 2. For both unmodified MOFs, Al-fum and MIL-53-TDC, the q_e values are lower than the water vapor uptake value measured previously by the volumetric method (Fig. 6) or calculated from the static humidity QCM measurements (ESI, Fig. S13†). The design of the QCM-based experiment does not allow us to take into account the moisture already trapped in the deposit at RH = 10% and the water that can be additionally adsorbed by a sample under a fog atmosphere if the equilibrium capacity is reached after a much longer exposure. Although the research on this topic is limited, the response of particulates to humid air (mass change, kinetics, hysteresis effect) is extremely sensitive to the sequence and the ratio of wet/dry relative humidity changes and the duration of each stage in a cyclic process.[89]

As one can see from Table 2, there is a 2–3 fold increase in the q_e value of Al fumarate/LbL powders as compared with the pristine MOF, although the mass fraction of polyelectrolytes in the composites is obviously less than 15% and the water absorption capacity of the LbL film material itself on planar surfaces is lower than the value for Al fumarate. Those are 220 ± 10 and 380 ± 10 mg g^{-1} for $(PSS/PDDA)_n$ and $(DexH/ChH)_n$ films, respectively,[52] against 450 ± 10 mg g^{-1} for the MOF. The enhanced water

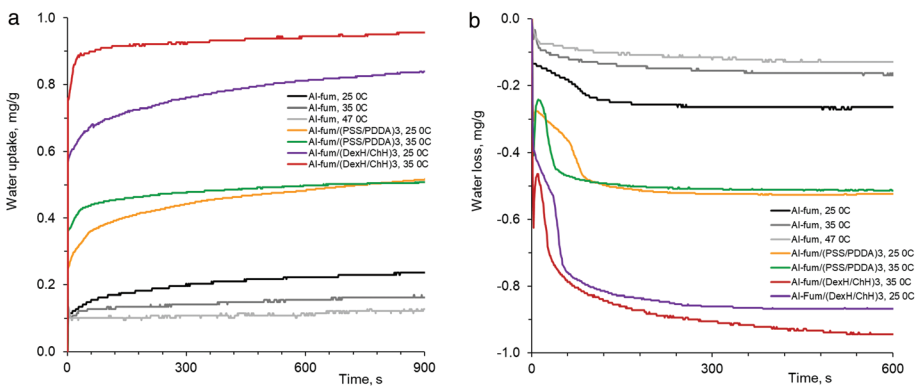

Fig. 7 Water uptake (a) and loss (b) *vs.* time curves of pristine Al-fum and modified with a $(PSS/PDDA)_3$ and $(DexH/ChH)_3$ shell as evaluated by QCM. In (b): the sharp drop of the curves within the first 20 s is due to the mechanical disturbance of the resonator after a rapid change of humid air in the measurement chamber.

Table 2 Parameters of water vapor adsorption/desorption by MOFs and MOF/LbL composites

MOF	Shell	T, °C	q_e, mg g^{-1}		q^a, mg g^{-1}	k^a, mg (g s)$^{-1}$	$t_{90\%}$, s		ΔR, Ohm
			Sorption	Desorption			Sorption	Desorption	
MIL-53-TDC	—	25	220 ± 20	200 ± 30	214 ± 29	199 ± 21	371 ± 18	71 ± 39	7–20
		35	110 ± 20	100 ± 10	110 ± 28	379 ± 85	231 ± 123	345 ± 95	0–1
		45	70 ± 10	60 ± 10	~55	>460	834 ± 191	618 ± 41	0–1
Al-fum	—	25	260 ± 20	280 ± 20	279 ± 15	49 ± 8	578 ± 99	105 ± 6	3–7
		35	170 ± 10	160 ± 10	173 ± 3	137 ± 51	409 ± 77	199 ± 22	0–1
		47	160 ± 20	160 ± 20	~141	>143	465 ± 62	294 ± 42	0–1
	$(PSS/PDDA)_3$	25	520 ± 20	550 ± 10	578 ± 33	47 ± 14	417 ± 72	89 ± 5	21–27
		35	500 ± 10	500 ± 10	514 ± 12	113 ± 24	100 ± 55	52 ± 2	9–11
	$(DexH/ChH)_3$	25	810 ± 40	880 ± 20	939 ± 99	36 ± 11	261 ± 22	61 ± 16	30–60
		35	980 ± 30	980 ± 30	986 ± 37	94 ± 22	23 ± 2	164 ± 13	25–30

[a] – calculated using the PSO model.

uptake by LbL coated powders is not completely due to the additive sorption by the shell material but is apparently caused by the changes introduced into the shape of the corresponding adsorption isotherm, namely, into the adsorption values before and after sharp incline at the inflection point and extra fast growth of adsorption in humid and fog atmosphere, similar to those found for other MOF/LbL composites (Fig. 6). It is assumed that the presence of the LbL shell changed the conditions of water vapor condensation at the particle–gas interface.

Moreover, for both investigated LbL shell compositions, the time period needed to reach 90% of the q_e value decreases as compared to that needed by Al fumarate; the drop is more pronounced at 35 °C than at lower temperatures (Table 2). In contrast to the unmodified sample, for which q_e decreases by ~35% when the temperature increases from 25 to 35 °C, water uptake by Al-fum/$(PSS/PDDA)_3$ is not affected by this temperature increase. However, for the Al-fum/$(DexH/ChH)_3$ powder, a 11% increase in the q_e value is observed as the temperature increases from 25 to 35 °C.

At 25 and 35 °C, water vapor sorption by both the neat Al-fum and MOF-53-TDC as well as their LbL composites can be approximated by a kinetic equation of the pseudo-second order (PSO) in its linear form:[52,90]

$$\frac{t}{q_t} = \frac{1}{k^* q^{*2}} + \frac{t}{q^*}$$

where t is time, s; q_t is the amount of adsorbed water at time t, mg g^{-1}; q^* is the amount of adsorbed water in equilibrium, mg g^{-1}, and k^* is the PSO constant, g (mg s)$^{-1}$. In the coordinates $\left(\frac{t}{q_t} - t\right)$, the kinetic curves are fitted by a linear function with a correlation coefficient higher than 0.995. The calculated values of q^* are in good agreement with the experimental q_e (Table 2). The calculated k^* reasonably rises with temperature.

As the temperature increases to 45–47 °C, water vapor adsorption accelerates as shown for Al fumarate (Fig. 7a) and is complete within a short time period that is shorter than the interval required for equilibrating the QCM resonator after injecting water vapor into the system. In this instance, only a lower limit of the constant was evaluated. Moreover, a weakly ascending part appears near the saturation point on the kinetic curves of both the MOFs that apparently reflects the changes in the nature of the adsorption sites.

The kinetics of water uptake by the bulk Al fumarate unmodified powder and the Al-fum/thick LbL composite with 50 wt% $(PSS/PDDA)_2$ shell evaluated on the basis of gravimetric measurements under real indoor conditions (23 °C, RH 70%) are shown in ESI, Fig. S14.† The saturation time of the composite also decreases similar to that for Al-fum/LbL deposits as found by QCM. The time changes from approximately 25 min for unmodified MOF to 15 min and 18 min in the 1st and 2nd humidity sorption cycles on the composite.

3.5 Apparent mechanism of LbL shell influence based on $\Delta F_t - \Delta R_t$ changes in the process of water uptake by MOF/LbL

A comparative analysis of water sorption and desorption by different MOF deposits on a quartz resonator in the (ΔR_t, ΔF_t) coordinates provides additional information on their structural transformations caused by alternately changing humidity. In the timeless coordinates, the process of water sorption by pristine Al fumarate is characterized by a linear dependence with a large negative $\Delta F_t/\Delta R_t$ slope (Fig. 8a), which is typical of rigid deposits.[60,91–98] A similar sharp decrease of the line in the (ΔR_t, ΔF_t) coordinates was obtained for MIL-53-TDC. The water desorption for pristine MOFs follows the same linear dependences as for adsorption just in the reversed direction.

At the same time, for LbL-coated Al fumarate powders, there are two pronounced sections on the ΔF_t *vs.* ΔR_t curves both for water uptake and desorption (Fig. 8b and c). The actual shapes of the curves depend on the temperature and structure of the shell but were observed for all the investigated Al-fum/LbL powders. We presume that the first section with a large negative $\Delta F_t/\Delta R_t$ slope corresponds to fast water suction into the MOF/LbL powder with a double-porous compartment structure. Due to the high rate and close sorption characteristics of the MOF and LbL shell materials, their individual contribution to the process remains indistinguishable. Previously, a large negative ΔF_t accompanied by almost zero ΔR_t has been observed in the process of the water vapor sorption into planar

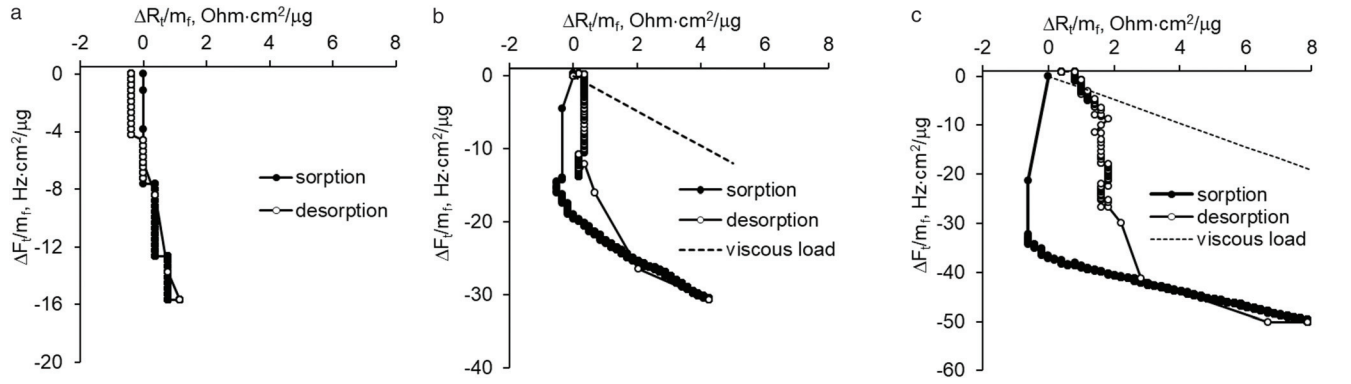

Fig. 8 ΔF_t *vs.* ΔR_t for water sorption (at RH 90%) and desorption (at RH 10%) by Al fumarate: unmodified (a); $(PSS/PDDA)_3$ (b), and $(DexH/ChH)_3$ (c). The 3rd cycle of humidity alternation. T = 25 °C.

$(PSS/PDDA)_n$ and $(ChH/DexH)_n$ films assembled on the surface of a QCM resonator.[52]

In the second stage of water uptake by Al-fum/LbL samples, ΔR_t increases considerably, while the $\Delta F_t/\Delta R_t$ slope declines. Ranging from −4.5 to −1.7 Hz Ohm^{-1}, the slope of the second stage fluctuates around the $\Delta F_t/\Delta R_t$ value for a typical viscous load (−2.4 Hz Ohm^{-1}).[97] The slow changes can be attributed to the rearrangement of the structure of fast wetted deposit accompanied by the formation of the meniscus of liquid water between the contacting particles and at the point of their contact with the resonator surface, and the involvement of repulsive forces between identically charged particles, resulting in a decrease in the strength of the deposit contact with the resonator surface and an increase in its porosity or viscosity. Based on the analysis of the $\Delta F_t - \Delta R_t$ curves within this stage, it is reasonable to assume some additional condensation of water in the stretched structure (for the MOF/LbL with $\Delta F_t/\Delta R_t$ < −2.4 Hz Ohm^{-1}) but not the formation of massive liquid film or droplets. In that case, the changes in the resonant frequency would be much larger and unlimited. The two-stage reversed process apparently involves flash evaporation of liquid water from menisci followed by water desorption from porous MOF/LbL microparticles.

The amplitude of R_t changes seems to diminish gradually with the increase in the number of water adsorption/desorption cycles (ESI, Fig. S12b†). This effect was observed for both uncoated MOFs, Al-fum and MIL-53-TDC, and MOF/LbL deposits. The changes can be explained in terms of the rearrangement of MOF particles in each wetting/dewetting cycle and a step-wise increase in the packing density of the deposit on the resonator surface.[98,99]

4. Conclusions

Water-stable metal–organic frameworks can be modified with a single polyelectrolyte layer or LbL shell without deterioration of their crystal structure which is responsible for the developed BET surface and high water uptake. Besides that, with the correct selection of shell composition and architecture, one can expect enhanced water sorption properties from the composite MOF/PE and MOF/LbL powders.

The selected hydrophilic MOFs are easily dispersed in water and their chemical structure does not deteriorate during the process of LbL assembly based on the adsorption of polyelectrolytes from their aqueous solutions. The PXRD analysis confirms that the crystal lattice parameters of the polyelectrolyte-coated MOF particles are identical to those of the unmodified powders. For the majority of MOFs coated with a single polyelectrolyte layer or one bilayer (two single layers) shell of negative and positive polyelectrolytes, no visual changes in the microparticle shape and size are found in the SEM microphotographs. If the LbL shell consists of 2 or 3 bilayers, the particles in the SEM images of the dry powder have well-defined boundaries and fairly close sizes. Simultaneously analyzing the MOF/PE suspensions by DLS, we found that during the process of sonication-assisted polyelectrolyte adsorption, MOFs with an average hydrodynamic diameter less than 700 nm tend to aggregate to varying degrees, while MOF bulk particles are slightly disintegrated or retain their size and polydispersity. The average diameter of original MOF powders varies from ~250 nm to 2.5 μm, while samples with only few coats show a diameter higher than 3.5 μm, which is associated with the aggregation of the dispersed phase by the polyelectrolyte.

By evaluating the ζ-potential changes upon step-wise addition of PSS, it was shown that the amount of polyelectrolyte needed to complete the layer of polymeric adsorbate on different MOFs is as low as 25 mg g^{-1}, it is 20 times lower than water typically absorbed by MOFs. Judging by the retention of high BET surface, overall water uptake parameters, and low shift of isotherm inflection, the adsorption of polyelectrolyte takes place predominantly on the surface of MOF particles regardless of their chemical and crystal structure. The only exceptions are polyelectrolytes with extremely low molecular weight, such as PAA and DexS. The mass percent of the polyelectrolyte material, therefore the thickness of the shell, was controlled by depositing the only polyelectrolyte layer as in MOF/PE (0.6–2.5 wt%), up to 3 bilayers as in MOF/LbL (<15 wt%) using the conventional LbL technique and applying the LbL technique without intermediate washing steps to accelerate the formation of a thick shell (50 wt%).

The core–shell structure and the related morphological changes of the MOF powders (aggregation of MOF particles by polyelectrolyte, partial disintegration by applied ultrasound, and the thin hydrophilic polymeric shell that uniformly enveloped each particle) make the water uptake characteristics of the MOF/PE and MOF/LbL powders unique. Under a constant relative pressure of water vapor, the moisture uptake by composite MOF/PE and MOF/LbL is rather comparable to that of pristine MOFs; this favorably distinguishes the core/shell composites from the matrix composites with conventional polymers, even highly hydrophilic ones.

The changes in the hydrophilicity/hydrophobicity of the surface by the adsorbed polyelectrolyte layers are well known. The hydrophilic surface promotes the formation of liquid menisci at the points of contact between particles.[100,101] The effect can apparently explain the higher values of water sorption than that of pristine MOFs by some MOF/PE at $0.3 < p/p_0 < 0.9$ on isotherms (Fig. 5), the increase in the water uptake by the Al-fum/$(PSS/PDDA)_3$ and Al-fum/$(DexH/ChH)_3$ powders under alternately changing humidity, and the slightly higher water moisture content of the MOF/LbL composite with a high mass percentage (~50 wt%) of the shell material. In the terms of changes in polyelectrolyte adsorption surfaces properties, a decrease in water sorption under an atmosphere with high humidity by some composites can be associated with an inhibition of liquid water condensation by more hydrophobic layers. Another advantage of the hydrophilic LbL shell coating on MOFs is that it accelerates moisture uptake and loss (Table 2).

Author contributions

Tatsiana Shutava: Conceptualization, investigation, methodology, visualization, writing – original draft, and review & editing. Christian Jansen: Investigation, data curation, formal analysis, visualization, and writing – original draft. Kanstantsin Livanovich: Investigation, methodology, and data curation. Vladimir Pankov: Conceptualization, funding acquisition, project administration, supervision, and writing – review & editing. Christoph Janiak: Conceptualization, funding acquisition, project administration, resources, supervision, validation, and writing – review & editing.

Conflicts of interest

There are no conflicts to declare.

Acknowledgements

This work was supported by grants 8.3.1.5 and 8.1.3.6 from the SPSR "Materials science, new materials and technologies" for 2021–2025, the Republic of Belarus.

References

1 D. M. Steinert, S.-J. Ernst, S. Henninger and C. Janiak, *Eur. J. Inorg. Chem.*, 2020, **2020**, 4502.
2 G. Maurin, C. Serre, A. Cooper and G. Férey, *Chem. Soc. Rev.*, 2017, **46**, 3104.
3 E. Hastürk, S.-J. Ernst and C. Janiak, *Curr. Opin. Chem. Eng.*, 2019, **24**, 26.
4 Q. Wang and D. Astruc, *Chem. Rev.*, 2020, **120**, 1438.
5 A. E. Baumann, D. A. Burns, B. Liu and V. S. Thoi, *Commun. Chem.*, 2019, **2**, 86.
6 K. Adil, Y. Belmabkhout, R. S. Pillai, A. Cadiau, P. M. Bhatt, A. H. Assen, G. Maurin and M. Eddaoudi, *Chem. Soc. Rev.*, 2017, **46**, 3402.
7 N. Stock and S. Biswas, *Chem. Rev.*, 2012, **112**, 933.
8 S.-T. Zheng, T. Wu, C. Chou, A. Fuhr, P. Feng and X. Bu, *J. Am. Chem. Soc.*, 2012, **134**, 4517.
9 M. Rubio-Martinez, C. Avci-Camur, A. W. Thornton, I. Imaz, D. Maspoch and M. R. Hill, *Chem. Soc. Rev.*, 2017, **46**, 3453.
10 B. J. Bucior, N.S. Bobbitt, T. Islamoglu, S. Goswami, A. Gopalan, T. Yildirim, O.K. Farha, N. Bagheri and R. Q. Snurr, *Mol. Syst. Des. Eng.*, 2019, **4**, 162.
11 D. Farrusseng, C. Daniel, C. Hamill, J. Casaban, T. Didriksen, R. Blom, A. Velte, G. Füldner, P. Gantenbein, P. Persdorf, X. Daguenet-Frick and F. Meunier, *Faraday Discuss.*, 2021, **225**, 384.
12 D. Lenzen, J. Zhao, S.-J. Ernst, M. Wahiduzzaman, A. K. Inge, D. Fröhlich, H. Xu, H.-J. Bart, C. Janiak, S. Henninger, G. Maurin, X. Zou and N. Stock, *Nat. Commun.*, 2019, **10**, 3025.
13 X. Liu, X. Wang and F. Kapteijn, *Chem. Rev.*, 2020, **120**, 8303.
14 M. P. Silva, A. M. Ribeiro, C. G. Silva, K. H. Cho, U.-H. Lee, J. L. Faria, J. M. Loureiro, J.-S. Chang, A. E. Rodrigues and A. Ferreira, *Sep. Purif. Technol.*, 2022, **290**, 120803.
15 D. Zhang, N. Luo, Z. Xue, Y.-L. Bai and J. Xu, *ACS Appl. Nano Mater.*, 2022, **5**, 2147.
16 H. Kim, S. R. Rao, E. A. Kapustin, L. Zhao, S. Yang, O. M. Yaghi and E. N. Wang, *Nat. Commun.*, 2018, 1191.
17 Y. Tu, R. Wang, Y. Zhang and J. Wang, *Joule*, 2018, **2**, 1452.
18 M. Wickenheisser and C. Janiak, *Microporous Mesoporous Mater.*, 2015, **204**, 242.
19 M. Wickenheisser, A. Herbst, R. Tannert and B. Milow, *Microporous Mesoporous Mater.*, 2015, **215**, 143.
20 M. Wickenheisser, T. Paul and C. Janiak, *Microporous Mesoporous Mater.*, 2016, **220**, 258.
21 V. Finsy, L. Ma, L. Alaerts, D. De Vos, G. Baron and J. Denayer, *Microporous Mesoporous Mater.*, 2009, **120**, 221.
22 D. Bradshaw, A. Garai and J. Huo, *Chem. Soc. Rev.*, 2012, **41**, 2344.
23 O.-L. Zhu and Q. Xu, *Chem. Soc. Rev.*, 2014, **43**, 5468.
24 E. Hastürk, S.-P. Höfert, B. Topalli, C. Schlüsener and C. Janiak, *Microporous Mesoporous Mater.*, 2020, **295**, 1909907.

25 E. Hastürk, C. Schlüsener, J. Quodbach, A. Schmitz and C. Janiak, *Microporous Mesoporous Mater.*, 2019, **280**, 277.
26 S. Gökpinar, S.-J. Ernst, E. Hastürk, M. Möllers, I. El Aita, R. Wiedey, N. Tannert, S. Nießing, S. Abdpour, A. Schmitz, J. Quodbach, G. Füldner, S. K. Henninger and C. Janiak, *Ind. Eng. Chem. Res.*, 2019, **58**, 2149.
27 R. G. Chaudhuri and S. Paria, *Chem. Rev.*, 2012, **112**, 2373.
28 J. Borges and J. F. Mano, *Chem. Rev.*, 2014, **114**, 8883.
29 M. Bruening and M. Adusumilli, *Mater. Matters*, 2011, **6**, 76.
30 G. Sukhorukov, in *Dendrimers, Assemblies, Nanocomposite, MML Series 5*, ed. R. Arshady and A. Guyot, Citus Books, London, 2002, ch. 4, pp. 111–147.
31 Y. Lvov, P. Pattekari and T. Shutava, in *Multilayer Thin Films: Sequential Assembly of Nanocomposite Materials*, ed. G. Decher and J. Schlenoff, Wiley-VCH, NY, London, 2012, ch. 8, pp. 151–170.
32 J. Sun, J. Li, D. Liu, Y. Ma and S. Yang, *Langmuir*, 2018, **34**, 6653.
33 R. Hlushko, J. F. Ankner and S. Sukhishvili, *Macromolecules*, 2021, **54**, 7469.
34 J. Ehrenmann, S. K. Henninger and C. Janiak, *Eur. J. Inorg. Chem.*, 2011, 471.
35 J. J. Richardson, J. Cui, M. Björnmalm, J. A. Braunger, H. Ejima and F. Caruso, *Chem. Rev.*, 2016, **116**, 14828.
36 J. Borges and J. F. Mano, *Chem. Rev.*, 2014, **114**, 8883.
37 Z. Zhang, J. Nong and Y. Zhong, *J. Neural Eng.*, 2015, **12**, 046015.
38 G. Cheng, C. Yin, H. Tu, S. Jiang, Q. Wang, X. Zhou, X. Xing, C. Xie, X. Shi, Y. Du, H. Deng and Z. Li, *ACS Nano*, 2019, **13**, 6372.
39 T. G. Shutava, K. S. Livanovich and V. V. Pankov, *Colloid. Surf. A.*, 2018, **539**, 69.
40 J. Lipton, G.-M. Weng, J. A. Röhr, H. Wang and A. D. Taylor, *Matter*, 2020, **2**, 1148.
41 C. Picart, *Curr. Med. Chem.*, 2008, **15**, 685.
42 S. B. Abbott, W. M. de Vos, L. L. E. Mears, R. Barker, R. M. Richardson and S. W. Prescott, *Macromolecules*, 2014, **47**, 3263.
43 V. Kozlovskaya, S. Harbaugh, I. Drachuk, O. Shchepelina, N. Kelly-Loughnane, M. Stone and V. V. Tsukruk, *Soft Matter*, 2011, **7**, 2364.
44 X. Liu and M. L. Bruening, *Chem. Mater.*, 2004, **16**, 351.
45 F. Vaca Chávez and M. Schönhoff, *J. Chem. Phys.*, 2007, **126**, 104705.
46 S.-W. Lee and D. Lee, *Macromolecules*, 2013, **46**, 2793.
47 C. Peniche-Covas, W. Argüelles-Monal and J. San Roman, *Polym. Int.*, 1995, **38**, 45.
48 J. E. Wong, F. Rehfeldt, P. Hänni, M. Tanaka and R. von Klitzing, *Macromolecules*, 2004, **37**, 7285.
49 M. Schönhoff, V. Ball, A. R. Bausch, C. Dejugnat, N. Delorme, K. Glinel, R. von Klitzing and R. Steitz, *Colloids Surf., A*, 2007, **303**, 14.
50 S. Dodoo, B. N. Balzer, T. Hugel, A. Laschewsky and R. von Klitzing, *Soft Matter*, 2013, **11**, 157.
51 V. Selin, J. F. Ankner and S. A. Sukhishvili, *Gels*, 2018, **4**, 7.
52 K. S. Livanovich, A.A. Bautramovich, V. V. Pankov and T. G. Shutava, *Polymer materials and technologies (Gomel)*, 2021, vol. 7, p. 50 (in russian).
53 B. D. Vogt, C. L. Soles, H.-J. Lee, E. K. Lin and W.-L. Wu, *Langmuir*, 2004, **20**, 1453.
54 A. Arce, F. Fornasiero, O. Rodriguez, C. J. Radke and J. M. Prausnitz, *Phys. Chem. Chem. Phys.*, 2004, **6**, 103.
55 L. Gao, C. Y. V. Li and K. Y. Chan, *Chem. Mater.*, 2015, **27**, 3601.
56 L. Gao, C. Y. V. Li, K. Y. Chan and Z. N. Chen, *J. Am. Chem. Soc.*, 2014, **136**, 7209.
57 H. Ejima, N. Yanai, J. P. Best, M. Sindoro, S. Granik and F. Caruso, *Adv. Mater.*, 2013, **25**, 5767.
58 S. Beyer, R. Schürmann, I. Feldmann, A. Blocki, I. Bald, R. J. Schneider and F. Emmerling, *Colloid Interface Sci. Commun.*, 2018, **22**, 14.
59 S. Liu, J. Chen, X. Bao, T. Li, Y. Ling, C. Li, C. Wu and Y. Zhao, *Chem. – Asian J.*, 2016, **11**, 1811.
60 T. G. Shutava, K. S. Livanovich and A. A. Sharamet, *Colloids Surf., B*, 2019, **173**, 412.
61 M. Thommes, K. Kaneko, A. V. Neimark, J. P. Olivier, F. Rodriguez-Reinoso, J. Rouquerol and K. S. W. Sing, *Pure Appl. Chem.*, 2015, **87**, 1051.
62 J. Landers, G. Y. Gor and A. V. Neimark, *Colloids Surf., A*, 2013, **437**, 3.
63 G. Sauerbrey, *Z. Phys.*, 1959, **155**, 206.
64 State Standard (GOST) 28237-89, *Test enclosures of non-injection type for constant relative humidity*, Standartinform Publ., Moscow, 2006.
65 S. H. Jhung, J.-H. Lee, J. W. Yoon, C. Serre, G. Férey and J.-S. Chang, *Adv. Mater.*, 2007, **19**, 121.
66 E. Leung, U. Müller, N. Trukhan, H. Mattenheimer, G. Cox and S. Blei, *US Pat*, 20120082864A1, 2011.
67 N. Tannert, S.-J. Ernst, C. Jansen, H.-J. Bart, S. K. Henninger and C. Janiak, *J. Mater. Chem. A*, 2018, **6**, 17706.
68 G. Zahn, H. A. Schulze, J. Lippke, S. König, U. Sazama, M. Fröba and P. Behrens, *Microporous Mesoporous Mater.*, 2015, **203**, 186.
69 G. C. Shearer, S. Chavan, J. Ethiraj, J. G. Vitillo, S. Svelle, U. Olsbye, C. Lamberti, S. Bordiga and K. P. Lillerud, *Chem. Mater.*, 2014, **26**, 4068.
70 F. Jeremias, D. Fröhlich, C. Janiak and S. K. Henninger, *RSC Adv.*, 2014, **4**, 24073.
71 K. H. Cho, P. G. M. Mileo, J. S. Lee, U.-H. Lee, J. Park, S. J. Cho, S. K. Chitale, G. Maurin and J.-S. Chang, *ACS Appl. Mater. Interfaces*, 2021, **13**, 1723.
72 P. Ghosh, Y. J. Colón and R. Q. Snurr, *Chem. Commun.*, 2014, **50**, 11329.
73 Y. Sun, A. Spieß, C. Jansen, A. Nuhnen, S. Gökpinar, R. Wiedey, S.-J. Ernst and C. Janiak, *J. Mater. Chem. A*, 2020, **8**, 13364.
74 T. J. M. M. Ntep, H. Reinsch, B. Moll, E. Hastürk, S. Gökpinar, H. Breitzke, C. Schlüsener, L. Schmolke, G. Buntkowsky and C. Janiak, *Chem. – Eur. J.*, 2018, **24**, 14048.

75 B. N. Dickhaus and R. Priefer, *Colloids Surf., A*, 2016, **488**, 15.
76 F. Hua, J. Shi, Y. Lvov and T. Cui, *Nanotechnology*, 2003, **14**, 453.
77 E. Kharlampieva, T. Tsukruk, J. M. Slocik, H. Ko, N. Poulsen, R. R. Naik, N. Kröger and V. V. Tsukruk, *Adv. Mater.*, 2008, **20**, 3274.
78 Z. Mao, L. Ma, C. Gao and J. Shen, *J. Controlled Release*, 2005, **104**, 193.
79 T. G. Shutava, P. P. Pattekari, K. A. Arapov, V. P. Torchilin and Y. M. Lvov, *Soft Matter*, 2012, **8**, 9418.
80 G. Bantchev, Z. Lu and Y. Lvov, *J. Nanosci. Nanotechnol.*, 2009, **9**, 396.
81 I. Teraoka, *Polymer Solutions: An Introduction to Physical Properties*, John Wiley & Sons, Inc., 2002.
82 A. Chatterjee and B. Das, *Carbohydr. Polym.*, 2013, **98**, 1297.
83 V. M. Prabhu, M. Muthukumara, G. D. Wignall and Y. B. Melnichenko, *Polymer*, 2001, **42**, 8935.
84 M. Nierlich, F. Boué, A. Lapp and R. Oberthur, *J. Phys. I*, 1985, **46**, 649.
85 H. M. Fares, Y. E. Ghoussoub, J. D. Delgado, J. Fu, V. S. Urban and J. B. Schlenoff, *Macromolecules*, 2018, **51**, 4945.
86 V. M. Prabhu, M. Muthukumara, G. D. Wignall and Y. B. Melnichenko, *J. Chem. Phys.*, 2003, **119**, 4085.
87 S. Despond, E. Espuche and A. Domard, *J. Polym. Sci., Part B: Polym. Phys.*, 2001, **39**, 3114.
88 R. Y. Aguiree-Loredo, A. I. Rodrigues-Hernandez and G. Velasquez, *Food Sci. Technol.*, 2017, **37**, 112.
89 R. Demir, S. Okur, M. Seker and M. Zor, *Ind. Eng. Chem. Res.*, 2011, **50**, 5606.
90 G. W. Kajjumba, S. Emik, A. Öngen, H. K. Özcan and S. Aydin, in *Advanced Sorption Process Applications*, ed. S. Edebali, IntechOpen, London, 2019.
91 K. A. Marx, T. Zhou, A. Montrone, H. Schulze and S. J. Braunhut, *Biosens. Bioelectron.*, 2001, **16**, 773.
92 M. C. Dixon, *J. Biomol. Tech.*, 2008, **19**, 151.
93 R. Lucklum and P. Hauptmann, *Electrochim. Acta*, 2000, **45**, 3907.
94 K. M. M. Aung, X. Ho and X. Su, *Sens. Actuators, B*, 2008, **131**, 371.
95 J. Iturri, A. C. Vianna, A. Moreno-Cencerrado, D. Pum, U. B. Sleytr and J. L. Toca-Herrera, *Beilstein J. Nanotechnol.*, 2017, **8**, 91.
96 R. Lucklum, *Electrochim. Acta*, 2000, **45**, 3907.
97 S. J. Martin, V. E. Granstaff and G. C. Frye, *Anal. Chem.*, 1991, **63**, 2272.
98 B. Acharya, C. M. Seed, D. W. Brenner, A. I. Smirnov and J. Krim, *Sci. Rep.*, 2019, **9**, 18584.
99 B. Du, A. M. König and D. Johannsmann, *New J. Phys.*, 2008, **10**, 053014.
100 S. D. N. Lourenço, D. Gallipoli, C. E. Augarde, D. G. Toll, P. C. Fisher and A. Congreve, *Géotechnique*, 2012, **62**, 193.
101 B. Torun, C. Kunze, C. Zhang, T. D. Kühne and G. Grundmeier, *Phys. Chem. Chem. Phys.*, 2014, **16**, 7377.